Huang et al. *Microsystems & Nanoengineering* (2025)11:231
https://doi.org/10.1038/s41378-025-01071-6

Microsystems & Nanoengineering
www.nature.com/micronano

ARTICLE Open Access

A high-precision nanoliter droplet dispensing system based on optoelectrowetting with tunable droplet volume

Kaicheng Huang[1], Zhen Liu[1], Yu Liu[1], Liming Deng[1], Luojia Jiang[1], Senlin Yan[1], Sijing Huang[1], Shuailong Zhang[2] and Xing Cheng[1]✉

Abstract

The capacity to generate high-precision droplets within Lab-on-a-Chip (LOC) devices is essential for numerous biochemical applications, such as DNA sequencing and drug delivery. In this study, we introduce an optoelectrowetting (OEW)-based droplet manipulation system that utilizes a novel droplet dispensing strategy, enabling precise nanoliter droplet dispensing with tunable droplet volume. The system comprises an OEW microchip, a liquid crystal display (LCD) projector connected to a laptop for generating customized light patterns, and a microscope equipped with a charge-coupled device (CCD) camera mounted above the OEW microchip for real-time observation. Simulations and experiments were conducted to investigate the optimal conditions for high-precision droplet dispensing. The system demonstrated exceptional stability in generating uniform droplets, with a minimum relative error (RE) of 0.45% and coefficient of variation (CV) of 2.49% for dispensing droplets of a volume of 36.52 nL. An experiment was conducted to dispense droplets of varying sizes, demonstrating the system's exceptional capability to generate droplets across a broad size range. The system was further validated through its application in polymerase chain reaction (PCR) amplification, confirming its performance in small-scale biochemical reactions. The results indicate that the proposed OEW droplet dispensing system is highly proficient in generating high-precision small-scale droplets with tunable volume. It also demonstrates its capability for biochemical processing and superior performance in sub-200 nL droplet dispensing compared to conventional pipetting techniques. This advancement holds significant potential for enhancing the performance and efficiency of LOC devices in biochemical research and clinical applications.

Introduction

Over the past few decades, droplet-based microfluidic systems have garnered significant research interest due to their broad utility in LOC applications[1,2]. These systems enable precise manipulation of discrete droplets containing biological or chemical reagents within immiscible phases, offering advantages over single-phase continuous flow, such as rapid mixing, minimized reagent dispersion, and reduced cross-contamination between droplets[3–5]. Consequently, droplet-based microfluidics has been successfully applied in cell encapsulation[6–8], microRNA detection[9,10], droplet array[11,12], droplet multiple displacement amplification (MDA)[13], and PCR[14,15]. However, a key limitation of these systems lies in the challenges associated with controlling individual droplets transported by continuous oil flow in microchannels[16].

To address these challenges, digital microfluidics (DMF) devices have been extensively developed and refined. DMF is an advanced liquid-handling technology that enables individual control of discrete droplets on an open-electrode array. These droplets, with volumes ranging from picoliters to microliters, serve as isolated reaction vessels and can be precisely manipulated to perform operations such as transport, merging, splitting, and

Correspondence: Xing Cheng (chengx@sustech.edu.cn)
[1]Materials Science and Engineering, Southern University of Science and Technology, Xueyuan Avenue, Shenzhen, 518055 Guangdong, China
[2]School of Integrated Circuits and Electronics, Beijing Institute of Technology, Beijing 100081, China

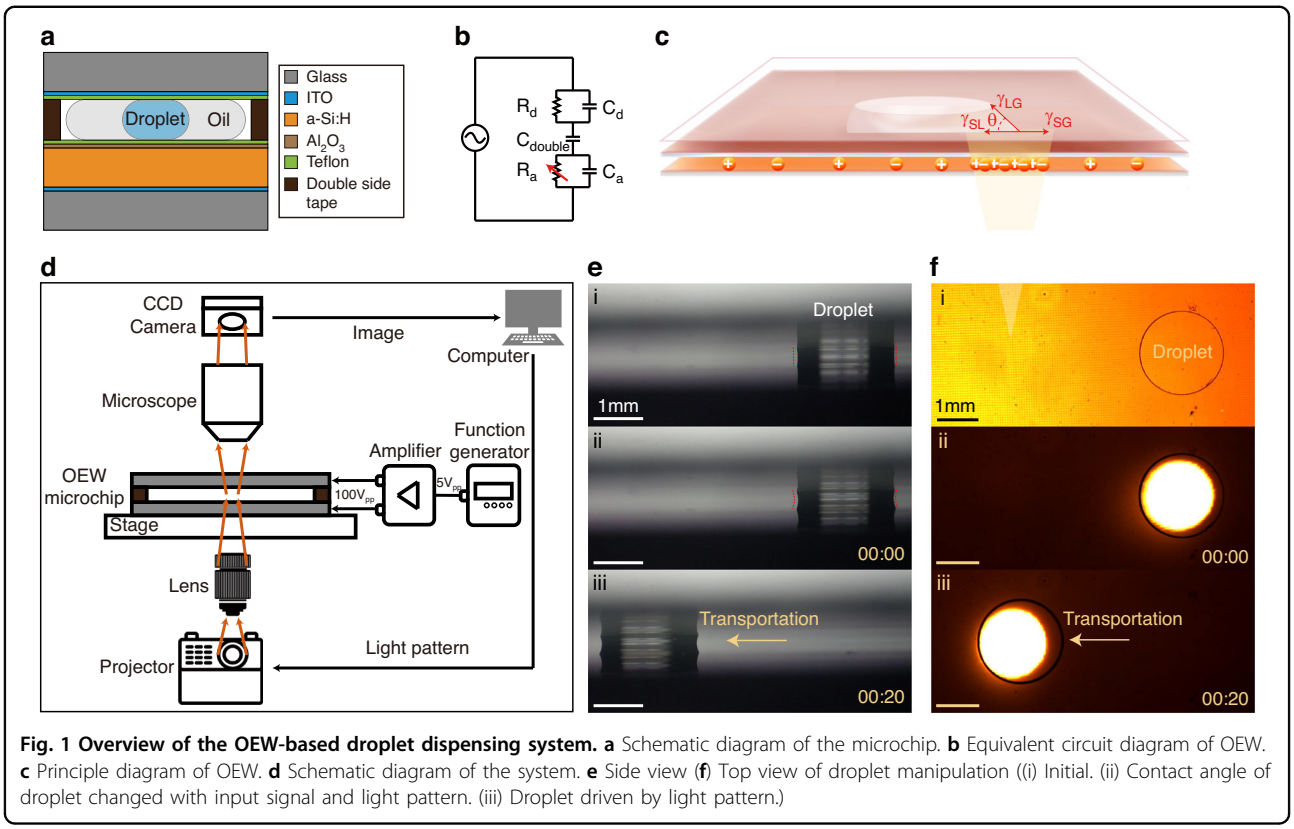

Fig. 1 Overview of the OEW-based droplet dispensing system. a Schematic diagram of the microchip. **b** Equivalent circuit diagram of OEW. **c** Principle diagram of OEW. **d** Schematic diagram of the system. **e** Side view (**f**) Top view of droplet manipulation ((i) Initial. (ii) Contact angle of droplet changed with input signal and light pattern. (iii) Droplet driven by light pattern.)

dispensing from reservoirs[17,18]. DMF actuation mechanisms include electrowetting-on-dielectric (EWOD)[19,20], magnetic actuation[21], and surface acoustic waves[22]. Among these, EWOD-based DMF has become the dominant approach due to its fast response time, simplified system architecture, and high precision[23]. The underlying principle, electrowetting (EW)[24], relies on voltage induced wettability modulation via embedded electrodes. When a voltage is applied, droplets deform and move due to the EW effect. By integrating large-scale microelectrode arrays, DMF devices enable programmable droplet manipulation with key advantages such as automation, addressability, system integration, and dynamic reconfigurability[23,25]. However, conventional fixed-electrode EWOD-DMF devices face fabrication challenges, including reliance on complex photolithography processes[26]. Additionally, the size and shape of the electrodes are fixed once the system is generated, which means the size of the droplet is limited. Furthermore, the number of electrodes is limited due to the complex control system for individual electrode control. Although thin-film transistor (TFT)-based EWOD systems have been explored[27–29], the integration of TFT-based microchip is complex, as their fabrication requires multiple micro- and nanofabrication processes, such as multi-layer overlay lithography, etching, and thin-film deposition.

A promising alternative is the development of lithography-free devices. Over the recent years, there has been a surge in scholarly inquiry into the optical modulation of the EWOD mechanism, an area of research denoted as OEW[30]. OEW offers several advantages over conventional EWOD, including simpler fabrication, reconfigurability, and enhanced flexibility. For droplet translation, localized electrode actuation is required to induce partial electrowetting of the droplet. Consequently, predefined electrodes is utilized in traditional EWOD-based chips, where electrode structure are preplanned and manufactured during the chip design phase, enabling individual electrode for droplet actuation. In contrast, the OEW mechanism builds upon traditional EWOD principles but incorporates a photoconductive layer (typically hydrogenated amorphous silicon, a-Si:H) between the dielectric layer and the bottom electrode (Fig. 1a). In OEW chips, the bottom electrode is a continuous, whole electrode without segmentation, rather than predefined electrodes. Upon illumination, localized changes in conductivity (Fig. 1b) induce contact angle modulation[30,31] (Fig. 1c). This phenomenon effectively creates a “virtual electrode,” which enables droplet actuation without the need for predefined physical electrodes. Therefore, OEW eliminates the need for complex electrode patterning and allows dynamic droplet control through light positioning[32,33]. With this

technique, the fabrication of an OEW microchip is more straightforward than that of an EWOD-based microchip, as it eliminates the need for overlay lithography and etching processes. While OEW provides greater flexibility than fixed-electrode EWOD, precise droplet manipulation remains challenging. Compared to droplet transportation, droplet generation (including splitting and dispensing from reservoir) is a more challenging process for EW devices[34]. Chiou et al.[35] initially employed OEW for droplet splitting and droplet dispensing from the reservoir. Park et al.[34] developed a single-sided continuous OEW system and successfully achieved 20 nL droplet splitting and 2.5 μL droplet dispensing from an external reservoir. Valley et al.[36] have built up a unified platform for OEW and optoelectronic tweezers (OET), where they realize 335 nL droplet splitting. Pei et al.[37] developed a continuous droplet dispensing strategy with a pair of reservoir light pattern and square light pattern (Supplementary Fig. 1). OEW enables the dispensing of arbitrarily shaped and sized droplets by modulating the light spot's dimensions and contours, offering unprecedented flexibility. However, the precision of the dispensing process remains uncontrollable and inconsistent. Despite the potential of OEW for applications, mathematical modeling and optimization still face significant challenges, considering the multitude of device and droplet parameters involved. The complex relationship between these variables and the resulting changes in contact angle and forces on the droplets requires thorough examination, as discussed in the literature[38].

Herein, we present an OEW-based droplet dispensing strategy that employs an optimized light pattern to achieve precise dispensing of nanoliter-scale droplets with tunable volume. An OEW-based droplet dispensing system was firstly constructed, as depicted in Fig. 1d. To visualize droplet behavior inside the microchannel under OEW actuation, a custom imaging module, comprising a horizontally aligned lens and a camera, was integrated to capture images of the droplet inside the channel. A simplified schematic is provided in Supplementary Fig. 2. Upon simultaneous application of the input signal and light pattern activation, the droplet contact angle is reduced by the OEW effect. This reduction is reflected in the top view image as an apparent thickening of the droplet edge (Fig. 1e, f(i, ii)). By controlling the position of the light pattern generated by the computer, the droplet within the microchip can be dynamically modulated, causing the droplet movement within the microchip (Fig. 1e. f(ii, iii)). The droplet dispensing procedure is shown in Fig. 2a, b. The effect of OEW would change the shape of the droplet, fitting the shape of the proposed light pattern. The introduction of necking in the light pattern would help the droplet form a controllable liquid bridge and shrink into a droplet filament (Fig. 2a, b(ii, iii), Fig. 2c), which is the natural form of a droplet when it is dispensed. The formation of the liquid bridge and droplet filament can eliminate the random factor of droplet dispensing, which is unregulated shrinkage and splitting. With the proposed light generation strategy, droplets can be precisely dispensed (Fig. 2d) and arranged into a droplet array (Fig. 2e).

The proposed OEW-based droplet dispensing system achieves high-precision nano-liter droplet generation, as demonstrated in Fig. 2f. In certain applications, such as drug discovery, a CV below 5% is typically required, while microdialysis applications demand even stricter precision with CV lower than 2%[39,40]. Most applications can be satisfied with a RE within 5%[39]. In this study, the minimum RE and CV for dispensing droplets of a volume of 36.52 nL were recorded at 0.45% and 2.49%, respectively, which significantly surpasses the required specifications. This precision is currently lower than that reported in previous OEW-based DMF studies[34,35,37] and most conventional EWOD-DMF systems[41–48]. Given the system's precise nano-liter droplet manipulation, the proposed OEW-based droplet dispensing system can be potentially applied in organ-on-chip platforms[49,50], offering a versatile tool for emerging microscale biochemical and toxicological investigations. Additionally, the proposed methods have enhanced the versatility of the DMF device for droplet dispensing, enabling high-precision dispensing across an exceptionally broad volume range, significantly expanding the operational capabilities of DMF devices.

Results

OEW microchip characterization

The operating principle of OEW relies on light-induced conductivity changes in the a-Si:H layer (Fig. 1c). When illuminated, the photoconductive layer modulates the interfacial wettability between the droplet and microchip surface. COMSOL simulations of electric potential were conducted to illustrate the principle of OEW. The COMSOL model comprises a 1 μm-thick a-Si:H photoconductive layer, a 100 nm-thick Al_2O_3 dielectric layer, a 1 μm-thick Teflon hydrophobic layer and a 100 μm-thick droplet layer. Figure 3a–c present finite-element simulations of the electric potential distribution on the surface between the a-Si:H layer and the Al_2O_3 layer with a droplet (circle) under various illumination conditions. Given that the droplet layer can be treated as a conductive layer and the potential difference across the droplet layer is relatively low (~0.01 V, Supplementary Fig. 3), the simulated electric potential on the surface between the a-Si:H layer and the Al_2O_3 layer is equivalent to the electric potential difference distribution across the dielectric layer (Al_2O_3 layer and teflon layer), which corresponds to the parameter ΔV in Eq. 4. In the absence of illumination (Fig. 3a), with a input voltage, the a-Si:H photoconductive layer exhibits high resistance,

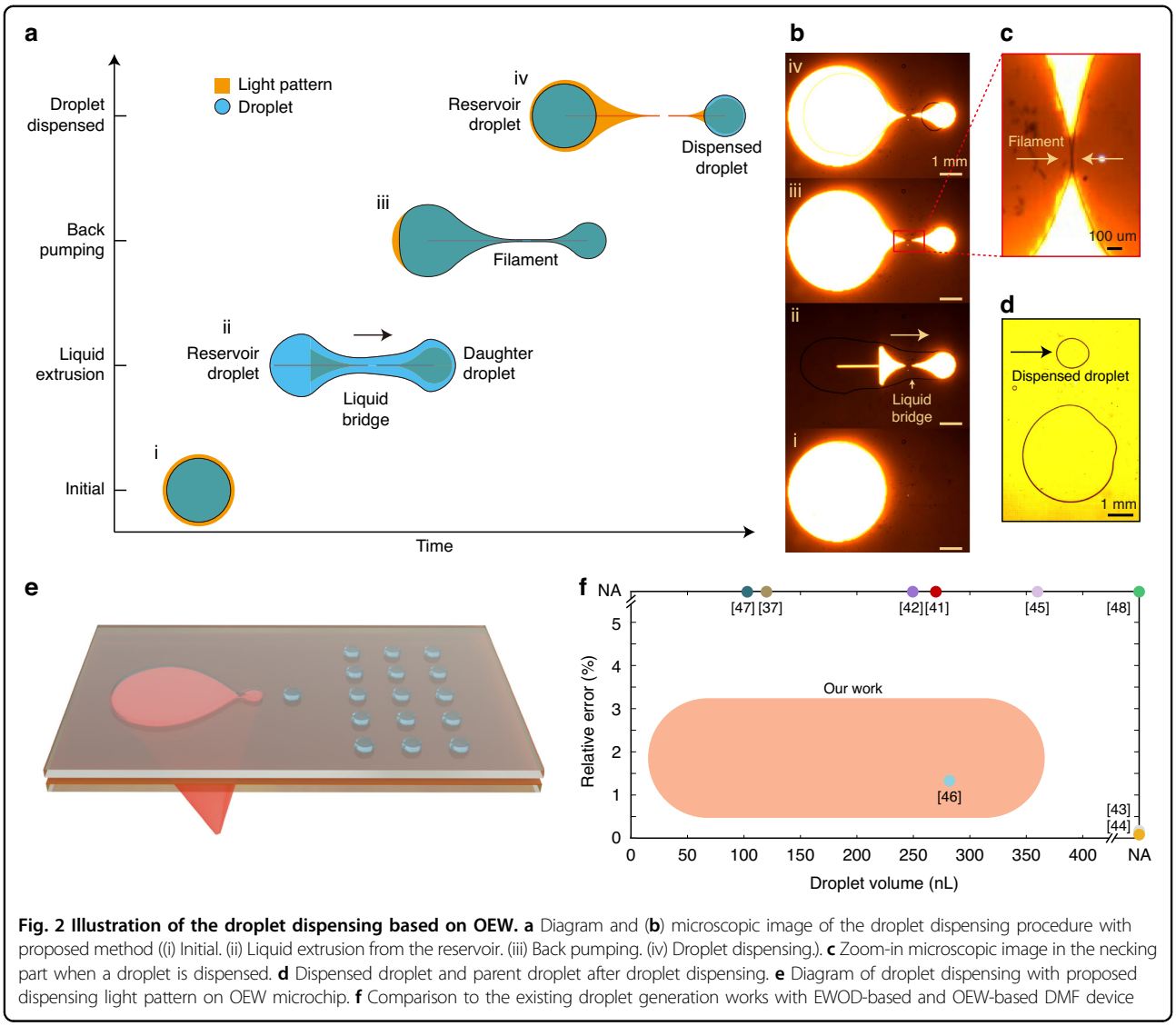

Fig. 2 Illustration of the droplet dispensing based on OEW. a Diagram and (**b**) microscopic image of the droplet dispensing procedure with proposed method ((i) Initial. (ii) Liquid extrusion from the reservoir. (iii) Back pumping. (iv) Droplet dispensing.). **c** Zoom-in microscopic image in the necking part when a droplet is dispensed. **d** Dispensed droplet and parent droplet after droplet dispensing. **e** Diagram of droplet dispensing with proposed dispensing light pattern on OEW microchip. **f** Comparison to the existing droplet generation works with EWOD-based and OEW-based DMF device

resulting in partial voltage application across the photoconductive layer and partial voltage application across the dielectric layer. Although the resulting uniform electrowetting force modulates the contact angle according to Eq. (5), the axisymmetric field preserves the circular footprint of the droplet in mechanical equilibrium. When the a-Si:H layer is uniformly illuminated across the droplet area (Fig. 3b), the photogenerated carriers in the illumination area dramatically increase the local conductivity of a-Si:H layer, collapsing the potential drop within the a-Si:H layer. The entire bias now appears across the dielectric layer, significantly enhancing the OEW effect. However, symmetric illumination does not induce droplet motion, as the droplet experiences identical electrowetting forces in all directions and the OEW effect remains uniform. When the light spot only partially covers the droplet (red area in Fig. 3c), the potential difference across the illuminated portion of the dielectric layer becomes larger than that across the non-illuminated portion. Consequently, the electrowetting force acting on the illuminated part of the droplet is stronger than that on the non-illuminated part, creating an unbalanced net force. As a result, the droplet migrates toward the illuminated region.

The OEW microchip was subjected to a characterization test to examine its OEW properties. A 10 nL droplet was dispensed onto the microchip surface, and its behavior was monitored using a horizontally aligned microscope-CCD imaging system. A circular light pattern was projected onto the OEW microchip to assess the impact of OEW. Figure 3d, e illustrate the state of a 10 nL droplet on the OEW microchip under a signal input of 110 V without and with illumination, respectively. The applied voltage induced contact angle modulation through the EWOD effect, which was significantly enhanced when a circular light pattern was projected onto the photoconductive

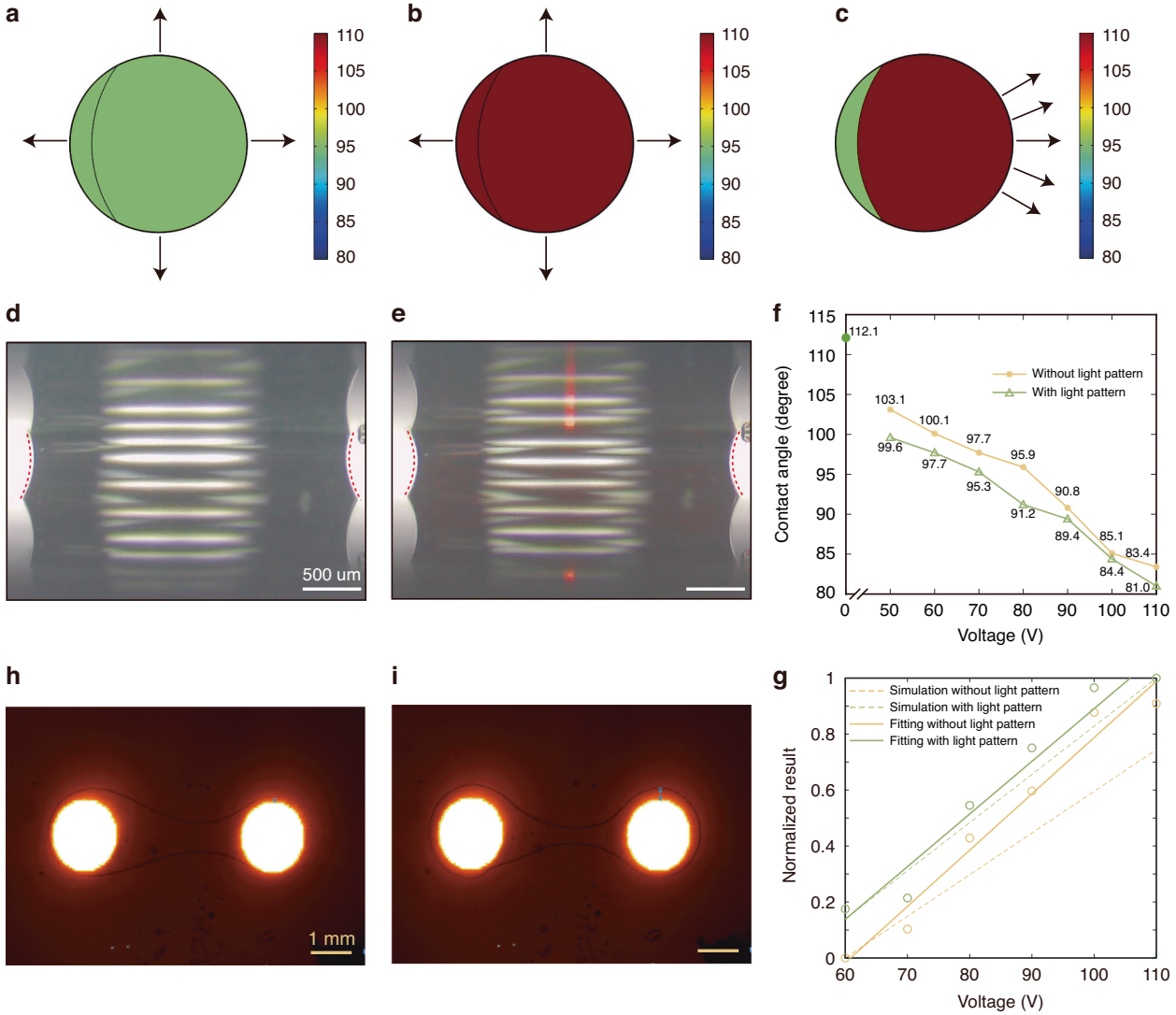

Fig. 3 Simulation and characterization of OEW microchip. COMSOL simulation of electric potential distribution on the surface between the a-Si:H layer and the Al2O3 layer with situation of (**a**) no light pattern, (**b**) with light pattern in the center of the droplet and (**c**) with a light pattern not in the center of the droplet. Side view picture of microchip characterization (**d**) without input voltage and (**e**) with an input voltage of 110 V. **f** Microchip characterization of contact angle versus input voltage with or without light pattern. **g** Normalized electric potential between the dielectric layer of the simulation result and the experimental result. Actuating range of the light pattern with a voltage of (**h**) 50 V and (**i**) 110 V

layer. The results of OEW microchip characterization are presented in Fig. 3f. The orange and green curve shows the data of contact angle in various voltages without and with a light pattern. In the initial, no voltage was applied to the microchip, and the contact angle was 112.1°. The introduction of the input signal changed the hydrophilic properties no matter if there is a light pattern. The change was enhanced with the increase in the voltage. OEW microchip exposed in a light pattern changed the concentration of photon-generated carrier in the a-Si:H, resulting in the increase of conductivity of the exposed area. Consequently, the OEW effect was significant under the light pattern. Figure 3g presents normalized simulation and experimental results, demonstrating excellent agreement in the voltage-dependent OEW response trends. This validation confirms the accuracy of the theoretical model in predicting the OEW behavior of the microchip.

Figure 3h, i present a static image of two circular light spots manipulating a droplet to determine the actuation range of the light pattern. Experiments were performed at voltages of 50 V and 110 V. A static equilibrium condition (Fig. 3h) is required to maintain droplet stability. The voltage gradient occurs along the periphery of the light pattern. An increase in voltage broadens the actuating scope of the light pattern. Consequently, to sustain a balanced state for the droplet enveloping the light pattern, the size of the

droplet would be enlarged, leading to a spontaneous shrinking of the liquid bridge as illustrated in Fig. 3i.

Dynamic droplet dispensing strategy

In conventional EWOD devices, droplets are dispensed without the implementation of a necking electrode, leading to an uncontrolled shrinking and pinch-off process. Additionally, the tail produced from the droplet necking would also influence the accuracy of dispensing the droplet. To address this, necking electrodes have been proposed[45,46]. Although the introduction of necking electrodes can assist in controlling the pinch-off location and mitigating tail-induced error, the accuracy of droplet dispensing remains constrained. This limitation arises because the rapid occurrence of the pinch-off procedure during the back-pumping step prevents the daughter droplet from conforming to the shape of the electrode.

To achieve precise droplet dispensing with OEW, a novel dynamic light-generation strategy is proposed in this study. The process of droplet dispensing with the proposed strategy can be delineated into three primary stages, as depicted in Fig. 2a, b. Initially, a reservoir droplet is illuminated and stabilized under a circular light spot to maintain its shape (Fig. 2a, b(i)). Upon deactivating this spot, a dispensing light spot with the necking light pattern is dynamically generated from the reservoir to extrude a daughter droplet from the reservoir (Fig. 2a, b(ii)). The extrusion is driven by competing EW and hydrophobic forces, with the former propelling the liquid forward while the latter expels it from the reservoir. In the meantime, a liquid bridge forms between the daughter droplet and the reservoir droplet owing to the liquid surface tension. Subsequently, a back-pumping step is initiated by re-energizing the original light spot, retracting the extruded droplet (daughter droplet and liquid bridge) (Fig. 2a, b(iii)). The back-pumping step enables the extruded droplet to conform to the shape of the light pattern, reshaping the daughter droplet into a circular form while shrinking the liquid bridge into an unstable filament ((Fig. 2a, b(iii)), c). Upon deactivation of the signal, the filament pinch-off, dispensing a daughter droplet ((Fig. 2a, b(iv)), Fig. d). Ideally, the dispensing of droplets with proper necking can attain a high degree of accuracy. While the back-pumping step effectively manipulates the droplet to fit the light pattern's contours, it may also precipitate a failed dispensing event. If the necking presented by the light pattern is excessively slender, the corresponding shrinking of the liquid bridge occurs rapidly, leading to a premature pinching before the droplet can fully conform to the light pattern (Supplementary Fig. 4a). This would result in an error between the intended dispensed droplet volume and the actual dispensed droplet volume. Conversely, if the necking in the light pattern is thick, the internal pressure within the droplet escalates, potentially retracting the daughter droplet back into the parent droplet and thwarting the dispensing process (Supplementary Fig. 4b). Hence, optimizing the light pattern is critical to balance these effects and ensure successful dispensing.

Given the critical role of the back-pumping phase in droplet dispensing accuracy, this study proposes an innovative light pattern to investigate the influence of necking geometry on the precision of droplet dispensing. As illustrated in Fig. 4a, a circular dispensing light spot is employed to extrude a daughter droplet, with the circular shape facilitating better conformity of the droplet to the light pattern. A necking light pattern follows the dispensing light spot, enabling the controlled shrinking and preventing unregulated shrinkage and splitting. During back-pumping, a circular original light spot is activated to retract the droplet, ensuring both the daughter droplet and the liquid bridge conform precisely to the light pattern's geometry. To ensure smooth transitions across the entire light pattern, the generation method for the light pattern is detailed in Supplementary Fig. 5. To systematically examine the relationship between light-pattern necking and dispensing precision, the fundamental light pattern is further modified. While OEW devices enable continuous droplet manipulation compared to conventional EWOD systems, the generated light patterns remain inherently discrete due to the digital nature of the projector. Consequently, minor pattern modifications may result in insufficient light-patterning precision, especially in the place where the filament occurs. To address this, the necking region is preserved but shortened, and a pair of configurable necking lights is integrated between the original and dispensing light spots, with adjustable thickness, length, and gap dimensions. Supplementary Fig.6 depicts the pressure analysis associated with the proposed light pattern for droplet dispensing. In accordance with the Laplace Equation, the pressure within the droplet, denoted as P, can be formulated based on the radius of curvature as follows:

$$P_d - P_a = \gamma\left(\frac{1}{r_d + R_d}\right) \tag{1}$$

$$P_o - P_a = \gamma\left(\frac{1}{r_o + R_o}\right) \tag{2}$$

$$P_n - P_a = \gamma\left(\frac{1}{r_n + R_n}\right) \tag{3}$$

where P_a is the atmospheric pressure. γ is the liquid surface tension coefficient. R represents the radius of curvature of the apex, and r is the main curvature radius,

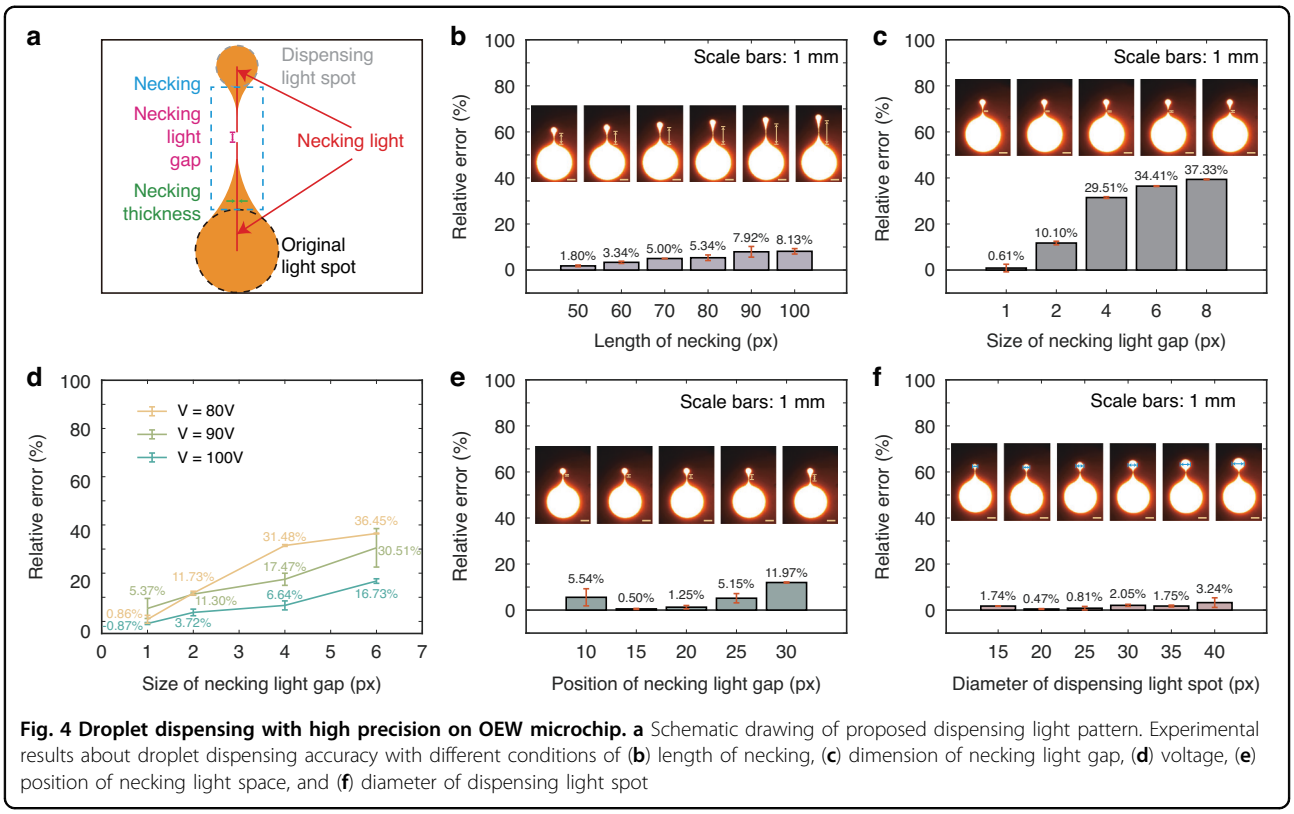

Fig. 4 Droplet dispensing with high precision on OEW microchip. a Schematic drawing of proposed dispensing light pattern. Experimental results about droplet dispensing accuracy with different conditions of (**b**) length of necking, (**c**) dimension of necking light gap, (**d**) voltage, (**e**) position of necking light space, and (**f**) diameter of dispensing light spot

which can be expressed by:

$$r = \frac{-d}{cos\theta_t + cos\theta_b} \tag{4}$$

where d represents the height of the gap, θ_b and θ_t represent the contact angle of the droplet on the upper plate and lower plate, respectively.

In contrast to conventional methods of droplet dispensing, the proposed high precision dispensing strategy necessitates a controllable decelerated shrinking and pinch-off process during the back-pumping step to achieve precise conformity between the droplet and light pattern. Consequently, the effect of necking on droplet dispensing was investigated through systematic adjustment of the necking light parameters.

Light pattern optimization

Systematic experiments were performed to characterize the effect of light pattern geometry on droplet dispensing accuracy. Critical parameters including the length of necking, dimension of necking light gap, applied voltage, necking light gap position, and dispensing light spot diameter were optimized to improve dispensing performance. Based on the experimental results, uniformly sized droplets were generated to validate system consistency, while droplets with varying dimensions were produced to assess dispensing flexibility.

Influence of length of necking

Upon dispensing, a liquid bridge would form, shrink and pinch off between the dispensed droplet and the reservoir. The residual portion of the liquid bridge transforms into the tail of the droplet, which is subsequently retracted back into the dispensed droplet due to the internal pressure. The presence of a tail during droplet dispensing is a significant factor contributing to reduced precision, as the tail is excluded from the calculation of the intended volume. Consequently, when dispensing smaller droplets, a larger RE would be observed, as the tail's size may become comparable to that of the dispensed droplet itself. Thus, the precision of dispensing droplets at a small scale is compromised by the influence of the tail.

This study investigates the correlation between necking length and RE to understand the tail's impact in conjunction with the length of necking, as depicted in Fig. 4b. Necking lengths below 50 pixels prevented successful droplet dispensing are therefore excluded. Experimental data revealed an inverse correlation between necking length and dispensing precision, with shorter necking lengths yielding improved accuracy. The results demonstrate that the incorporation of the necking effectively

reduces the RE associated with the tail, as the necking light pattern is integrated into the intended volume. This integration ensures that the precision of droplet dispensing at the nanoliter scale can be reliably achieved. However, the light pattern and the droplet do not perfectly overlap, leading to increased relative error with longer necking. Hence, a minimum necking length of 50-pixel short was adopted for the subsequent experimental trials.

Influence of dimension of necking light gap

As discussed in the previous section, the premature pinching-off of the droplet filament is known to escalate the RE in droplet dispensing. To minimize this error, the present study introduces a pair of necking lights. The dimension of the gap between the necking lights was investigated, given its significant correlation with the shrinking and pinching procedure of the droplet filament. Figure 4c illustrates the relationship between the dimension of the necking light gap and the RE. The image illustrations above correspond to various experimental conditions. It is observed that an enlargement of the gap between the necking lights corresponds to an increment in relative error. This suggests that the shrinking of the droplet filament is accelerated with an increased gap in the necking light, thereby promoting the pinching-off procedure of the droplet filament before the droplet fully conforms to the shape of the light pattern. Based on these findings, a gap size of 1 pixel was adopted in the light generation strategy. This approach allows for a controlled space for the filament to contract while simultaneously circumventing the rapid pinching off.

Influence of voltage

Voltage represents a critical parameter that can influence the shrinking behavior of the liquid bridge. Although voltage does not directly dictate the droplet filament's shrinkage, it is intimately connected to the actuating scope of the light pattern.

Based on the microchip characterization presented in the previous section (Fig. 3h, i), increasing the voltage expands the actuation range of the light pattern, inducing spontaneous shrinking of the liquid bridge. It reveals that higher voltages tend to promote liquid bridge shrinkage. However, the introduction of necking light leads to an inverse outcome. The necking light serves to prevent the shrinking of the liquid bridge, effectively stabilizing the liquid bridge adjacent to the light, thus preventing the liquid bridge from shrinking into a droplet filament and premature pinch-off. Figure 4d illustrates the relationship between the dimension of the necking light gap and the RE with varying voltage inputs. Voltages ranging from 80 V to 100 V were tested, as it was determined that a voltage lower than 80 V is insufficient to drive the droplet, while a voltage exceeding 100 V risks damaging the dielectric layer. The data indicate that an increased voltage reduces RE, as a higher voltage enhances the stabilizing effect of the necking light. This enhancement ensures that the droplet filament is preserved in the back-pumping step, providing sufficient time for the droplet to conform to the shape of the light pattern. Based on these findings, a maximum voltage of 100 V was selected as the optimal operating voltage for subsequent experiments.

Influence of position of necking light gap

Given the significant role of the droplet tail in affecting the precision of droplet dispensing, their effects warrant systematic investigation. The necking has been designed in two parts to facilitate the study of both the dimension of the necking light gap and the length of the tail. By controlling the length of each necking segment, the shrinking and pinching position of the droplet filament can be designed, as exemplified in the images presented in Fig. 4e. Upon the cessation of the input signal, the pinch-off procedure happens at the location where the filament shrink, resulting in tails of varying lengths.

In prior sections, the pinch-off point of the droplet filament was positioned midway through the necking to achieve halving. In this section, the gap of the necking light has been adjusted to investigate the influence of tail length on droplet dispensing. A similar result has been observed compared to the influence of the length of necking, that a shortened tail would reduce the RE for droplet dispensing. However, there is a threshold for shortening the tail that the pressure from the dispensing light spot has to be enough to hold the daughter droplet. Otherwise, the back-pumping procedure would retract the daughter droplet as discussed and increase the RE. Therefore, the gap of the necking light has been adjusted to approximate the dispensed light spot, which in this case is 15 pixels.

Influence of diameter of dispensing light spot

To evaluate the versatility of the proposed system in dispensing droplets of varying sizes, following the optimization of the light pattern, an experiment aimed to ascertain the correlation between the diameter of the dispensing light spot and the resultant RE was conducted. Within the scope of this study, diameters above 15 pixels were examined, as a dispensing light spot with a diameter of <15 pixels would lead to an unsuccessful dispensing process due to insufficient droplet pressure.

Figure 4f presents the precision results of dispensing droplets of varying sizes. The data indicate that diminishing the size of the dispensing light spot concurrently reduces the necking size, thereby minimizing the error associated with necking. However, when the size of the dispensing light spot falls below a critical threshold (20

pixels in this case), the pressure exerted by the dispensing light spot becomes insufficient to maintain the stability of the daughter droplet, culminating in a heightened relative error. Even so, the system achieves a RE below 5% for droplet dispensing with light spot diameters ranging from 15−40 pixels, meeting the precision threshold discussed in the previous section. These results demonstrate the versatility of the proposed system for high-precision droplet dispensing across a broad size range.

Droplet dispensing performance

The performance of the system was evaluated through experimental procedures utilizing the optimized light pattern. 0.2% Tween-20 solution was employed for droplet dispensing. The system's stability was first assessed by dispensing droplets of uniform size in an array with an automation program. A dispensed light spot with a diameter of 20 pixels was set as depicted in Fig. 5a. Subsequently, the dispensed droplets were transferred and stabilized using a circular light pattern, culminating in the formation of a droplet array as shown in Fig. 5b. Ultimately, the proposed light generation strategy successfully produced a 2×10 droplet array, with the dispensed droplets exhibiting a mean volume of 36.52 nL (Fig. 5c). The CV and RE values were recorded at 2.49% and 0.45%, respectively, showing the stability and accuracy of the proposed system.

Furthermore, a flexibility test was conducted to ascertain the system's capability in dispensing droplets of diverse sizes. Dispensed light spots with diameters ranging from 20−70 px were utilized to generate droplets of varying sizes, as illustrated in Fig. 5d, e. The dispensed droplets were also driven and maintained by a circular light pattern.

The dispensed droplets were organized into a 2×3 array, as shown in Fig. 5f. Results confirm the capability of the proposed system for accurate droplet dispensing across a wide size range, highlighting its versatility. The relationship between the input radius and the output droplet volume of dispensed droplets with different sizes is shown in Supplementary Fig. 7. It is observed that the dispensed droplet volume exhibits an almost linear relationship with the square of the input radius. This indicates that the tail of the droplet has only a slight significance to the overall volume of the dispensed droplet.

Plasmid DNA amplification

To validate the applicability of the proposed system for biochemical reactions, it was used to dispense primer solution for accomplishing plasmid DNA amplification. Primer solution droplets of varying volumes were generated using light patterns with dispensing light spot diameters ranging from 20 to 40 pixels. Pipette was also used to achieve droplet dispensing for accomplishing plasmid DNA amplification to compare the on-chip droplet dispensing result and off-chip manually pipette result (Fig. 5h). The fitting curve for off-chip amplification data and on-chip amplification data shows that the proposed droplet dispensing strategy presents the same performance for droplet dispensing as the pipette. Moreover, the proposed system can achieve smaller-scale droplet dispensing compared to the existing pipette, filling the gap of droplet dispensing under 200 nL with the pipette. Figure 5i, j shows the electrophoresis result for PCR amplification with the proposed droplet dispensing system and a manual pipette respectively. It can be seen that both experiments share the same electrophoresis bands, verifying the PCR experiment results. To eliminate the potential impact of primers on the experimental results, a negative control group lacking a template was also established. This control group was used to assess the influence of primers on absorbance. The result is shown in Supplementary Fig. 8. It can be seen that the primer band is distinct from the band of the target plasmid DNA product. Therefore, the influence of primers on the original experimental results can be ruled out. These results validate our system as a reliable alternative to manual pipetting for small-volume biochemical applications.

Discussion

The growing demand for precise biochemical reactions and cost-effective pharmaceutical applications has precipitated a significant demand for high-accuracy droplet dispensing systems. In this research, an OEW microchip has been integrated with a programmable light-patterning system and a novel light generation strategy to achieve high-precision droplet dispensing. The microchip was loaded with water-in-oil droplets at first to optimize system performance. Image processing methodologies were engaged to extract dimensional information for the light pattern and dispensed droplet. A digital projector dynamically generated and projected customizable light patterns onto the microchip, enabling precise droplet actuation according to the prescribed optical fields. Consequently, the droplets on the microchip could be driven with the intended shape of the light pattern. A series of experiments was executed to identify the optimal light pattern, enhancing the precision of the system for droplet dispensing. Then, an experiment was conducted to dispense droplets of uniform size. The system demonstrated exceptional stability in generating uniform droplets ($CV = 2.49\%$, $RE = 0.45\%$). This was achieved through the precise control and replication of droplet dispensing, which is indicative of the system's reliability and consistency in operation. Subsequently, an additional experiment was performed to dispense droplets of varying sizes, thereby showcasing the system's capability to accurately dispense droplets across a spectrum of sizes

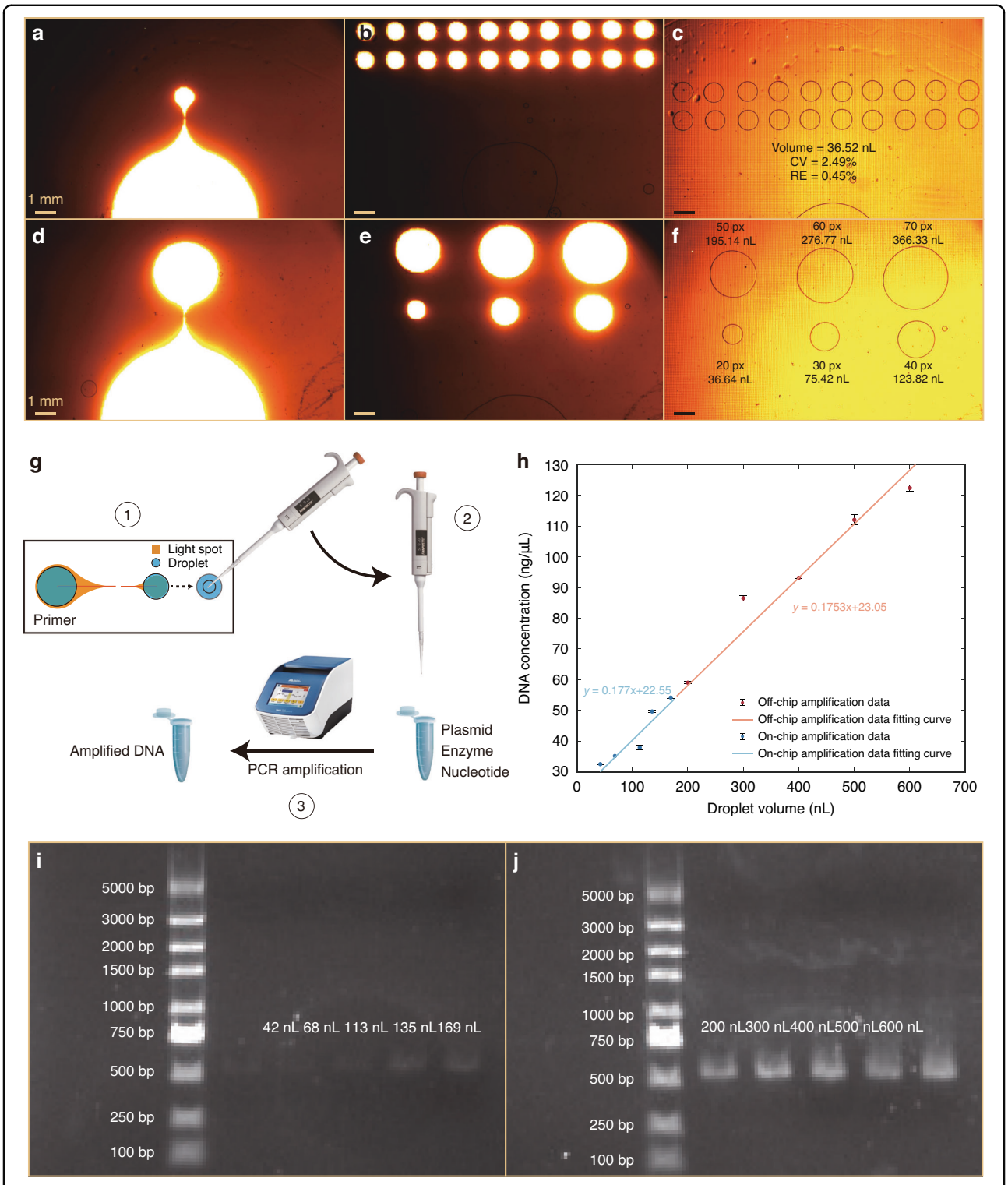

Fig. 5 Results of dispensing droplets of uniform size. a The initial light pattern for droplet dispensing. **b** The final light pattern for holding the droplets in the same size. **c** The result of dispensing droplets in an array of 2 × 10. Results of dispensing droplets of varying sizes. **d** The initial light pattern for droplet dispensing. **e** The final light pattern for holding the droplets in different sizes. **f** The result of dispensed droplets in an array of 2 × 3 with different sizes. **g** Experimental procedure for PCR amplification with proposed droplet dispensing system. **h** Experimental result for PCR amplification with the proposed droplet dispensing system (Blue) and manual pipette (orange). Electrophoresis result for PCR amplification with (**i**) proposed droplet dispensing system, and (**j**) a manual pipette

with high precision. This experiment underscores the system's remarkable flexibility in producing droplets across a wide size range (20−70 pixels in diameter). The proposed system introduces a flexible and high-precision approach through the utilization of OEW for droplet dispensing. Finally, the proposed system was used to achieve primer solution droplet dispensing for accomplishing plasmid DNA amplification, demonstrating both its capability for biochemical processing and superior performance in sub-200 nL droplet dispensing compared to conventional pipetting techniques. These results address a critical gap in small-volume liquid handling. Our OEW-based approach offers distinct advantages for droplet manipulation. Given the operational similarities between OEW and TFT-based EWOD systems, these findings suggest potential applicability of our droplet dispensing strategy in TFT-based EWOD platforms. This could enable new possibilities for high-precision digital microfluidics, particularly in pharmaceutical and life science applications where droplet consistency and accuracy are critical.

Materials and methods

Principle of OEW

The investigation into EW as a robust technique for controlling minute volumes of liquid has been extensive since Lippmann's pioneering work in 1875[24]. When an electric potential is applied across the interface of a liquid droplet and a solid electrode, it triggers a reconfiguration of the electric charges, thereby modifying the surface tension at the liquid-solid boundary. The contact angle (θ) adopted by a liquid droplet can be precisely calculated using the Lippmann-Young equation, expressed as follows:

$$cos\theta + cos\theta_0 + \frac{c_d(\triangle V)^2}{2\gamma_{LG}} \quad (5)$$

where θ_0 denotes the initial contact angle of the droplet when no electric potential is applied, γ_{LG} refers to the interfacial surface tension between two immiscible fluids, specifically the liquid droplet and the surrounding medium, c_d signifies the capacitance per unit area of the dielectric layer, while ΔV represents the voltage change, or the potential difference, across the dielectric capacitor.

Design of the OEW system

The core element of the system is the OEW microchip, configured in a sandwich-style architecture as depicted in Fig. 1a. The upper plate is a transparent indium tin oxide (ITO) glass, spin-coated with a 100 nm Teflon film, which functions as a hydrophobic surface. The lower plate is designed as a light-reactive functional layer. The lower plate is composed of five distinct layers, sequentially from the base to the top: a glass substrate, an ITO layer, an a-Si:H layer, an aluminum oxide (Al_2O_3) layer, and a Teflon layer. The ITO glass and the Teflon layer perform similar roles to those in the upper plate. The a-Si:H layer acts as a photoconductive surface, with its conductivity increasing upon exposure to light. The Al_2O_3 layer with a thickness of 100 nm acts as a dielectric layer, shielding the majority of the voltage applied to the droplet and preventing electrical breakdown. Situated between the upper and lower plates is a 70 μm-thick double-sided tape, serving as a spacer. The ITO glass is a commercially available product. The 1 μm a-Si:H layer was deposited using plasma-enhanced chemical vapor deposition (PECVD). The 100 nm Al_2O_3 layer was deposited via atomic layer deposition (ALD). The 100 nm Teflon layer was applied by the spin-coating method (1000 r/min, 30 s). Detail fabrication process is presented in Supplementary Fig. 9

The complete system is illustrated in Fig. 1d. Positioned atop the microchip is a CCD camera coupled with a microscope, designed to capture image information. A projector and lens assembly are placed at the base of the microchip to produce the requisite light patterns. A computer interfaced with the CCD camera receives the visual input and directs the projector to create the desired light patterns. A function generator paired with an amplifier is linked to the ITO layers in both the upper and lower plates, supplying an alternating current signal to the microchip. Supplementary Fig. 10 presents an actual photograph of the entire system setup.

Materials in the experiment

Experimental droplet medium preparation

To demonstrate the system's capability in droplet dispensing, deionized (DI) water containing Tween 20 at a volumetric concentration of 0.2% was utilized at first. Decamethyltetrasiloxane, a type of silicone oil, was selected as the immiscible fluid injected into the channel enveloping the droplet, as it allows the droplets to be propelled with ease within the oil medium.

Plasmid DNA preparation

Plasmid DNA preparation was performed using Escherichia coli (E. coli). Specifically, 5 μL of plasmid DNA was mixed with 50 μL of E. coli cell medium. To promote the uptake of plasmid DNA into the bacterial cells, the mixture was subjected to a brief heat shock treatment at 42 °C for 90 s. Subsequently, the medium was placed in an ice-water bath for 10 min to reduce the membrane permeability of E. coli. The processed E. coli cells were then incubated with lysogeny broth (LB) culture medium at 37° C for 17 h. Following incubation, the plasmid DNA was extracted using the Mag-MK Plasmid DNA Mini-Preps Kit (Sangon Biotech).

Experimental protocol

Droplet dispensing

DI water with 0.2% Tween 20 was dripped on the lower plate with a volume of 1.5 μL. The upper plate, affixed with two strips of double-sided tape, was covered on the lower plate to form a microchannel measuring 70 μm in height. Subsequently, silicone oil was injected into the channel, enveloping the applied droplet. Utilizing the proposed droplet dispensing strategy, the successful dispensing of daughter droplets can be achieved.

Plasmid DNA amplification

The plasmid DNA amplification procedure is illustrated in Fig. 5g. A primer solution containing 0.2% Tween 20 was prepared. A 1.5 μL droplet of the primer solution was dispensed into the OEW microchip, serving as a reservoir droplet. With the optimized light generation strategy, droplets of various volumes were dispensed using light patterns with diameters of the dispensing light spot ranging from 25−45 pixels. The dispensed droplets were then transported to an open hole drilled in the upper plate. Using a pipette, the droplet was transferred to a centrifuge tube containing 0.1 μL of plasmid DNA, 2 μL of sterilized ddH_2O and 2.5 μL of SanTaq Plus PCR Mix (Sangong Biotech) (including enzyme and nucleotide). The mixture was subsequently subjected to PCR amplification. The quantity of amplified DNA was measured using the Invitrogen Qubit 4 Fluorometer (Thermo Fisher). Additionally, the amplified DNA was processed through DNA gel electrophoresis to determine the size of the amplified DNA fragments.

Evaluation of inconsistency and precision

To evaluate the system's stability and precision, two key factors have been investigated. One is the CV, which is defined as the ratio of the standard deviation to the mean of the droplet radius. In this study, the area of the droplet is used for measurement, given that the droplet with the dispersant would not maintain a uniform circular shape in its natural state, and the radius of the droplet is hard to define. Therefore, the CV is expressed as follows:

$$CV = \frac{S_{std}}{S_{mean}} \times 100\% \tag{6}$$

where S_{std} represents the standard deviation of the dispensed droplet area, while S_{mean} denotes the mean of the dispensed droplet area. This metric provides a quantitative measure of the stability in droplet size, which is crucial for assessing the performance of the droplet dispensing system.

The precision of droplet volume is characterized by the degree of conformity between the actual area of the dispensed droplet and the intended area. Greater volume precision equates to a lower margin of error. Here, the inaccuracy is measured by the RE, which reflects the difference between the average area of repeatedly generated droplets and the intended area. In this research, the intended area is manipulated by adjusting the area of the light pattern. Consequently, the RE is calculated using the subsequent formula:

$$RE = \frac{S_{mean-}S_{light}}{S_{light}} \times 100\% \tag{7}$$

where S_{light} is the area of the dispensed light pattern. This formula provides a quantitative measure of the system's accuracy in dispensing droplets of the intended volume.

Acknowledgements
This work was financially supported in part by Guangdong-Hong Kong-Macau Joint Laboratory on Micro-Nano Manufacturing Technology (Grant No. 2021LSYS004), National Natural Science Foundation of China (Grant No. 62403231), National Natural Science Foundation of China (Grant No. 31927802) and Shenzhen Science and Technology Innovation Commission (Grant No. RCJC20200714114436046).

Author contributions
Conceptualization: K.C.H., X.C. Methodology: K.C.H., Z.L., Y.L., XC. Investigation: K.C.H., Z.L., L.M.D., S.L.Y., S.J.H. Visualization: K.C.H., YL. Supervision: S.L.Z., X.C. Writing—original draft: K.C.H. Writing—review and editing: K.C.H., Y.L., S.L.Z., X.C.

Competing interests
The authors declare no competing interests.

Supplementary information The online version contains supplementary material available at https://doi.org/10.1038/s41378-025-01071-6.

Received: 21 April 2025 Revised: 16 September 2025 Accepted: 16 September 2025
Published online: 28 November 2025

References

1. Chen, L. et al. Ultra-sensitive fluorescence-activated droplet single-cell sorting based on tetramer-hcr-evagreen amplification. *Microsyst. Nanoeng.* **11**, 10 (2025).
2. Shen, S. et al. A reflective display based on the electro-microfluidic assembly of particles within suppressed water-in-oil droplet array. *Light Sci. Appl.* **12**, 290 (2023).
3. Wang, J., Wang, J., Feng, L. & Lin, T. Fluid mixing in droplet-based microfluidics with a serpentine microchannel. *RSC Adv.* **5**, 104138–104144 (2015).
4. Olzmann, J. A. & Carvalho, P. Dynamics and functions of lipid droplets. *Nat. Rev. Mol. Cell Biol.* **20**, 137–155 (2019).
5. Park, S.-Y., Wu, T.-H., Chen, Y., Teitell, M. A. & Chiou, P.-Y. High-speed droplet generation on demand driven by pulse laser-induced cavitation. *Lab Chip* **11**, 1010–1012 (2011).
6. Lee, J. M. et al. Generation of tumor spheroids using a droplet-based microfluidic device for photothermal therapy. *Microsyst. Nanoeng.* **6**, 52 (2020).
7. Headen, D. M., Garc´ıa, J. R. & Garc´ıa, A. J. Parallel droplet microfluidics for high throughput cell encapsulation and synthetic microgel generation. *Microsyst. Nanoeng.* **4**, 1–9 (2018).
8. Tang, T., Zhao, H., Shen, S., Yang, L. & Lim, C. T. Enhancing single-cell encapsulation in droplet microfluidics with fine-tunable on-chip sample enrichment. *Microsyst. Nanoeng.* **10**, 3 (2024).
9. Tong, Z. et al. All-in-one multiple extracellular vesicle miRNA detection on a miniaturized digital microfluidic workstation. *Biosens. Bioelectron.* **270**, 116976 (2025).
10. Tong, Z. et al. Rapid automated extracellular vesicle isolation and miRNA preparation on a cost-effective digital microfluidic platform. *Anal. Chim. Acta* **1296**, 342337 (2024).

11. Feng, H. et al. Massive electro-microfluidic particle assembly patterns in droplet array for information encoding. *Small* **20**, 2405161 (2024).
12. Feng, H. et al. Microwell confined electro-coalescence for rapid formation of high-throughput droplet array. *Small* **19**, 2302998 (2023).
13. Kim, S. C. et al. Measurement of copy number variation in single cancer cells using rapid emulsification digital droplet MDA. *Microsyst. Nanoeng.* **3**, 1–7 (2017).
14. Qu, Y. et al. Non-invasive detection of tumor markers in salivary extracellular vesicles based on digital PCR chips. *Clin. Chim. Acta* **548**, 117488 (2023).
15. Yin, H. et al. Ultrafast multiplexed detection of SARS-CoV-2 RNA using a rapid droplet digital PCR system. *Biosens. Bioelectron.* **188**, 113282 (2021).
16. Frey, C., G¨opfrich, K., Pashapour, S., Platzman, I. & Spatz, J. P. Electrocoalescence of water-in-oil droplets with a continuous aqueous phase: implementation of controlled content release. *ACS omega* **5**, 7529–7536 (2020).
17. Choi, K., Ng, A. H., Fobel, R. & Wheeler, A. R. Digital microfluidics. *Annu. Rev. Anal. Chem.* **5**, 413–440 (2012).
18. Guo, K. et al. An artificial intelligence-assisted digital microfluidic system for multistate droplet control. *Microsyst. Nanoeng.* **10**, 138 (2024).
19. Miller, E. M. & Wheeler, A. R. A digital microfluidic approach to homogeneous enzyme assays. *Anal. Chem.* **80**, 1614–1619 (2008).
20. Wheeler, A. R. Putting electrowetting to work. *Science* **322**, 539–540 (2008).
21. Cheng, H., Liu, H., Li, W. & Li, M. Recent advances in magnetic digital microfluidic platforms. *Electrophoresis* **42**, 2329–2346 (2021).
22. Seo, J. et al. Path-programmable water droplet manipulations on an adhesion-controlled superhydrophobic surface. *Sci. Rep.* **5**, 12326 (2015).
23. Xu, X. et al. Digital microfluidics for biological analysis and applications. *Lab Chip* **23**, 1169–1191 (2023).
24. Lippmann, G. et al. Relations entre les ph´enom'enes ´electriques et capillaires. *Ann. Chim. Phys.* **5**, 494–549 (1875).
25. Li, J., Ha, N. S., Liu, T., Dam, R. M. & Kim, C.-J. Ionic-surfactant-mediated electrodewetting for digital microfluidics. *Nature* **572**, 507–510 (2019).
26. Shen, H.-H., Fan, S.-K., Kim, C.-J. & Yao, D.-J. Ewod microfluidic systems for biomedical applications. *Microfluidics Nanofluidics* **16**, 965–987 (2014).
27. Zhan, S. et al. Implementing an AC signal driving in digital microfluidic chips with active-matrix thin-film transistors. In *IEEE Sensors Journal*, 33922—33928 (IEEE, 2024)
28. Jia, Z. et al. Artificial intelligence enabled multipurpose smart detection in active-matrix electrowetting-on-dielectric digital microfluidics. *Microsyst. Nanoeng.* **10**, 139 (2024).
29. Wang, D. et al. Active-matrix digital microfluidics design for field programmable high-throughput digitalized liquid handling. *Iscience* **27**, 109324 (2024).
30. Chiou, P. Y., Moon, H., Toshiyoshi, H., Kim, C.-J. & Wu, M. C. Light actuation of liquid by optoelectrowetting. *Sens. Actuators A Phys.* **104**, 222–228 (2003).
31. Thio, S. K. & Park, S.-Y. A review of optoelectrowetting (oew): from fundamentals to lab-on-a-smartphone (los) applications to environmental sensors. *Lab Chip* **22**, 3987–4006 (2022).
32. Wang, T. et al. Intelligent optoelectrowetting digital microfluidic system for real-time selective parallel manipulation of biological droplet arrays. *Lab Chip* **25**, 1416—1428 (2025)
33. Wu, T. et al. Investigation into the optoelectrowetting droplet transport mechanism. *Electrophoresis* **45**, 1428–1442 (2024).
34. Park, S.-Y., Teitell, M. A. & Chiou, E. P. Single-sided continuous optoelectrowetting (scoew) for droplet manipulation with light patterns. *Lab Chip* **10**, 1655–1661 (2010).
35. Chiou, P.-Y., Chang, Z. & Wu, M. C. Droplet manipulation with light on optoelectrowetting device. *J. Microelectromech. Syst.* **17**, 133–138 (2008).
36. Valley, J. K., NingPei, S., Jamshidi, A., Hsu, H.-Y. & Wu, M. C. A unified platform for optoelectrowetting and optoelectronic tweezers. *Lab Chip* **11**, 1292–1297 (2011).
37. Pei, S. N., Valley, J. K., Wang, Y.-L. & Wu, M. C. Distributed circuit model for multicolor light-actuated opto-electrowetting microfluidic device. *J. Lightwave Technol.* **33**, 3486–3493 (2015).
38. Strassner, J., Doering, C., Oliveira, E. & Fouckhardt, H. Optoelectrowetting (oew) with push-actuation of microdroplets at small frequencies and oew equations revisited. *Sens. Actuators A Phys.* **334**, 113331 (2022).
39. Rose, D. Microdispensing technologies in drug discovery. *Drug Discov. Today* **4**, 411–419 (1999).
40. Ren, H., Fair, R. B. & Pollack, M. G. Automated on-chip droplet dispensing with volume control by electro-wetting actuation and capacitance metering. *Sens. Actuators B Chem.* **98**, 319–327 (2004).
41. Cho, S. K., Moon, H. & Kim, C.-J. Creating, transporting, cutting, and merging liquid droplets by electrowetting-based actuation for digital microfluidic circuits. *J. Microelectromech. Syst.* **12**, 70–80 (2003).
42. Kremers, T., Thelen, S., Bosbach, N. & Schnakenberg, U. Portadrop: A portable digital microfluidic platform providing versatile opportunities for lab-on-a-chip applications. *PLoS ONE* **15**, 0238581 (2020).
43. Nikapitiya, N. J. B., Nahar, M. M. & Moon, H. Accurate, consistent, and fast droplet splitting and dispensing in electrowetting on dielectric digital microfluidics. *Micro Nano Syst. Lett.* **5**, 1–10 (2017).
44. Nikapitiya, N.J.B., You, S.M. & Moon, H. Droplet dispensing and splitting by electrowetting on dielectric digital microfluidics. In *2014 IEEE 27th International Conference on Micro Electro Mechanical Systems (MEMS)*, 955—958 (IEEE, 2014).
45. Wang, W., Chen, J. & Zhou, J. An electrode design for droplet dispensing with accurate volume in electro-wetting-based microfluidics. *Appl. Phys. Lett.* **108**, 243701 (2016).
46. Wang, H. & Chen, L. Novel electrodes for precise and accurate droplet dispensing and splitting in digital microfluidics. *Nanotechnol. Rev.* **10**, 857–869 (2021).
47. Wang, W., Jones, T. & Harding, D. On-chip double emulsion droplet assembly using electrowetting-on-dielectric and dielectrophoresis. *Fusion Sci. Technol.* **59**, 240–249 (2011).
48. Jin, K. et al. " One-to-three" droplet generation in digital microfluidics for parallel chemiluminescence immunoassays. *Lab Chip* **21**, 2892–2900 (2021).
49. Wang, Y. et al. Revealing transport, uptake and damage of polystyrene microplastics using a gut-liver-on-a-chip. *Lab Chip* **25**, 1656–1668 (2025).
50. Wang, L. et al. Gut-on-a-chip for exploring the transport mechanism of Hg (ii). *Microsyst. Nanoeng.* **9**, 2 (2023).